Journal of Electrical and Computer Engineering Innovations
(JECEI)
Journal homepage: http://www.jecei.sru.ac.ir

Research paper

Torque Ripple Reduction by Using Virtual Vectors in Direct Torque Control Method Using Neutral-Point-Clamped Inverter

H. Afsharirad [*]***, S. Misaghi***

Department of Electrical Engineering, Azarbaijan Shahid Madani University, Tabriz, Iran.

Article Info

Article History:
Received 06 August 2024
Reviewed 26 September 2024
Revised 25 October 2024
Accepted 14 November 2024

Keywords:
Multi-level inverter
Neutral-point-clamped inverter
Direct torque control
Permanent magnet synchronous motor
Voltage vector
Virtual vector

Corresponding Author's Email Address:
h.afsharirad@azaruniv.ac.ir

Abstract

Background and Objectives: Due to the high torque ripple and stator current harmonics in direct torque control using a two-level inverter, the use of multi-level inverters has become common to reduce these two factors. Among the multilevel inverters, the Neutral-point-Clamped Inverter has been given more attention in the industry due to its advantages. This inverter has 27 voltage vectors by which torque and flux are controlled. In order to reduce torque ripple and current harmonic as much as possible, methods such as space vector modulation methods or the use of multi-level inverters with higher levels have been considered. But the main drawback of these methods is the increase of complexity and cost.
Methods: In this article, virtual voltage vectors are used to increase the number of hysteresis controller levels. These vectors are obtained from the sum of two voltage vectors. In this way, we will have 12 voltage vectors in addition to the diode clamped inverter's voltage vectors. Therefore, we can increase the number of torque hysteresis levels from 7 levels to 11 levels.
Results: Considering that the proposed method uses virtual vectors and voltage vectors, it does not increase the cost and computational complexity. Also, one of the requirements of using this method is the use of fixed switching frequency, which solves the variable switching frequency problem of conventional methods. Therefore, the proposed control reaches an overall optimization.
Conclusion: To verify the feasibility of the proposed method and compare it with the conventional method, both of these methods are simulated in the MATLAB /Simulink environment and the simulation results represent the efficiency of the proposed control method. This method achieves less torque ripple and harmonic current without increasing the cost and computational complexity.

Introduction

Direct torque control (DTC) is one of the practical motor drive system controllers. This controller advantages include no need for other reference frame transforms, very simple structure, high transient response and its robustness. This controller directly controls flux and torque with a hysteresis controller, choosing best voltage vector in each area to reach and control flux and torque [1]-[3] However, DTC has disadvantages like high torque and flux ripple [4], [5].

One method to reduce torque ripple and current harmonics is using multilevel inverters. Multilevel inverters, besides mentioned advantages, benefit from reduced switching frequency, reduced switching losses, and reduced voltage stress on switches [6]-[8]. Multilevel inverters classify into several categories based on structure, with most important being Neutral-Point-Clamped Inverter (NPCI), flying capacitor inverters, H-

bridge inverters, and cascaded inverters.

NPCIs widely used in industry due to advantages. Its advantages include easier bidirectional power transfer capability, use at all voltage levels, and simpler structure [9]-[12]. Various methods propose to further improve these inverters' performance in reducing torque ripple. These methods include using modulation techniques in DTC, using virtual vectors, or using other control methods like model predictive controller [13]-[17]. In [18], a NPCI controls a five-phase induction motor. This paper uses a modulation method calculating switching time in switching period using two voltage vectors for switching, reducing transient states. In [19], a NPCI controls a permanent magnet synchronous motor (PMSM), where duty cycle calculation reduces torque and flux ripple. In [20], PWM uses for induction motor control, improving motor performance. However, a 60-pulse converter supplies the inverter for improved power quality. In [21], a NPCI uses for PMSM control, where duty cycle calculates for inverter switching. This method improves motor performance, reducing torque and flux ripple. In [22], switching time of two voltage vectors in switching interval adjusts, and a torque regulator replaces hysteresis controller, increasing control system efficiency. In [23], a NPCI uses for PMSM drives, employing two voltage vectors in duty cycle. Duty cycle calculation method minimally depends on motor parameters. These control methods with PMSM enhance control system advantages and stability. PMSM, due to their benefits, are main rivals to induction motors. Among these benefits are high power density, compact size, low copper losses from lacking rotor windings, and simple structure [24]-[29].

Conventional methods typically employ either direct torque control based on lookup tables or duty cycle calculation with multiple voltage vectors applied within a duty cycle period. In lookup table-based approaches, switching frequency varies, and some methods don't utilize the inverter's full capacity, using medium-amplitude voltage vectors to reduce torque ripple even when larger vectors are needed. For instance, paper [30], an example of a conventional duty cycle-based method, uses medium voltage vectors in scenarios requiring large voltage vectors. The proposed method in this paper uses fixed switching frequency for direct torque control, resolving the variable switching frequency issue.

Conversely, duty cycle calculation methods often use virtual voltage vectors without considering the sufficiency of the inverter's voltage vector. For example, reference [21] employs three voltage vectors for motor control in each duty cycle period, which is unnecessary in some intervals. The proposed method not only considers the number of voltage vectors in hysteresis bands but also maximizes inverter capability, using only one voltage vector in these bands. Additionally, in hysteresis bands with low torque ripple amplitude, an appropriate voltage vector is applied, and in some intervals, two voltage vectors are used for better torque variation response.

To prevent significant increases in switching frequency, the proposed method considers voltage vectors of previous and subsequent levels. When using a virtual voltage vector, only one voltage vector is employed to generate it. This approach effectively addresses the limitations of conventional methods while optimizing inverter performance and torque control.

The paper innovates by increasing hysteresis controller levels without adding switches to enhance voltage vectors. Traditionally, multilevel inverters reduce torque ripple in direct torque control of two-level inverters by increasing voltage vectors. A two-level inverter has 8 voltage vectors, while a diode-clamped inverter has 27, each with unique amplitudes and angles.

This method, instead of increasing voltage levels, sums voltage vectors to create new vectors with different amplitudes and angles from the main ones, applied based on torque hysteresis levels. This approach increases voltage vectors to 39, achieving more vectors and hysteresis levels without additional switches, thus reducing torque ripple and current harmonics.

The method necessitates fixed switching frequency, an advantage over conventional variable-frequency hysteresis controllers. This fixed frequency approach marks a significant improvement from traditional techniques. By combining vector summation and fixed frequency, the paper presents a novel solution for enhancing inverter performance without increasing system complexity, addressing key limitations in existing direct torque control methods.

Different sections here are: Section 2 discuss about technical work preparation. Section 3 presents simulation results, and Section 4 provides conclusions.

Technical Work Preparation

A. The Conventional Direct Torque Control Method Using a NPCI

The NPCI, due to advantages, is one of industry's most widely used inverters. Fig. 1 shows three-phase three-level inverter. As seen in this figure, each inverter leg has 4 power electronic switches and 2 diodes, with each power electronic switch connected to DC link through a diode. Each switch in this inverter represents by symbol Skfn, where k corresponds to phase number {A, B, C}, f indicates switch position {p for positive, N for negative}, and n specifies switch number.

Table 1 illustrates switching pattern for one inverter leg. As inferred from this table, if ‘Sap1’ and ‘Sap2’ turn on, voltage +vdc/2 produces at inverter output. If switch ’Sap1’ and ‘San1’ on, inverter output voltage is 0. If ‘San1’ and ‘San2’ turn on, voltage -vdc/2 produces at inverter output.

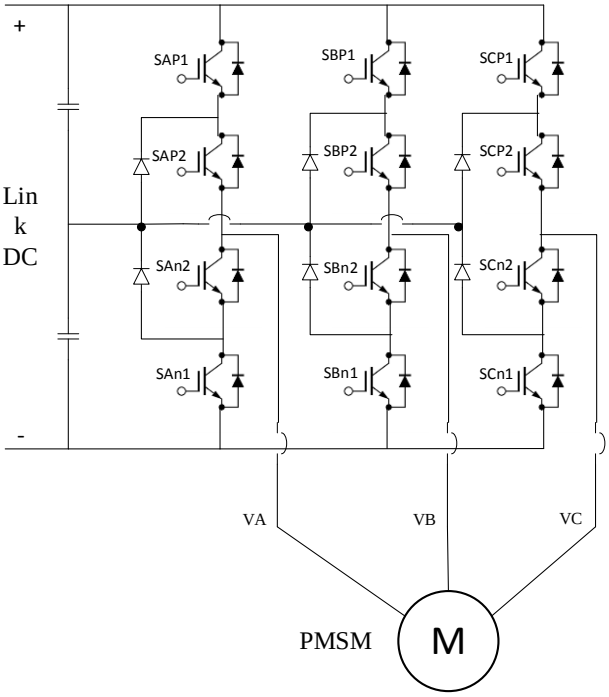

Fig. 1: Three-phase, three-level diode clamped inverter.

Table1: Switching table of NPCI

SAp1	SAp2	SAn1	SAn2	Phase Voltage
On	On	Off	Off	*Vdc*/2
Off	On	On	Off	0
Off	Off	On	On	-*Vdc*/2

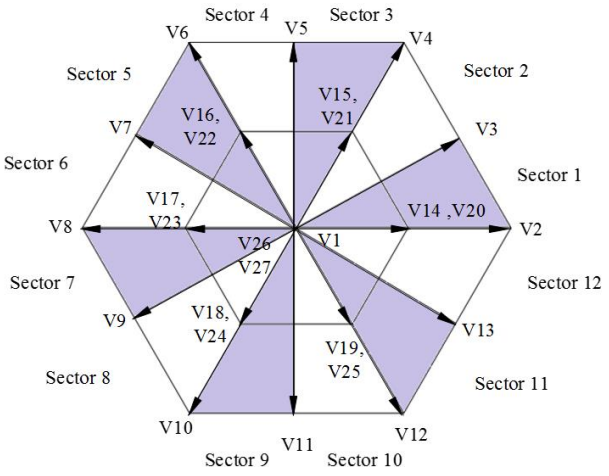

Fig. 2: Distribution of voltage vectors in the αβ plane.

Table 2 shows voltage vectors of three-phase three-level diode-clamped inverter. This table displays 27 voltage vectors resulting from this inverter. State '1' corresponds to respective switch being turned on, while state '0' corresponds to switch being turned off. Additionally, Fig. 2 illustrates distribution of voltage vectors in αβ plane.

Table 2: Diode clamped inverter's voltage vectors

Switches of inverter						VV	$\lvert\overline{V_s}\rvert$	angle
S_{Ap1}	S_{Ap2}	S_{Bp1}	S_{Bp2}	S_{Cp1}	S_{Cp2}			
0	0	0	0	0	0	$\overline{V_1}$	0	-
1	1	0	0	0	0	$\overline{V_2}$	$Vdc\sqrt{2/3}$	0
1	1	0	1	0	0	$\overline{V_3}$	$Vdc\sqrt{1/2}$	$\pi/6$
1	1	1	1	0	0	$\overline{V_4}$	$Vdc\sqrt{2/3}$	$\pi/3$
0	1	1	1	0	0	$\overline{V_5}$	$Vdc\sqrt{1/2}$	$\pi/2$
0	0	1	1	0	1	$\overline{V_6}$	$Vdc\sqrt{2/3}$	$2\pi/3$
0	0	1	1	0	1	$\overline{V_7}$	$Vdc\sqrt{1/2}$	$5\pi/6$
0	0	1	1	1	1	$\overline{V_8}$	$Vdc\sqrt{2/3}$	π
0	0	0	0	1	1	$\overline{V_9}$	$Vdc\sqrt{1/2}$	$7\pi/6$
0	0	0	0	1	1	$\overline{V_{10}}$	$Vdc\sqrt{2/3}$	$4\pi/3$
0	1	0	0	1	1	$\overline{V_{11}}$	$Vdc\sqrt{1/2}$	$3\pi/2$
1	1	0	0	1	1	$\overline{V_{12}}$	$Vdc\sqrt{2/3}$	$5\pi/3$
1	1	0	0	0	1	$\overline{V_{13}}$	$Vdc\sqrt{1/2}$	$11\pi/6$
1	1	0	1	0	1	$\overline{V_{14}}$	$Vdc\sqrt{1/6}$	0
1	1	1	1	0	1	$\overline{V_{15}}$	$Vdc\sqrt{1/6}$	$\pi/3$
0	1	1	1	0	1	$\overline{V_{16}}$	$Vdc\sqrt{1/6}$	$2\pi/3$
0	1	1	1	1	1	$\overline{V_{17}}$	$Vdc\sqrt{1/6}$	π
0	1	0	1	1	1	$\overline{V_{18}}$	$Vdc\sqrt{1/6}$	$4\pi/3$
1	1	0	1	1	1	$\overline{V_{19}}$	$Vdc\sqrt{1/6}$	$5\pi/3$
0	1	0	0	0	0	$\overline{V_{20}}$	$Vdc\sqrt{1/6}$	0
0	1	0	1	0	0	$\overline{V_{21}}$	$Vdc\sqrt{1/6}$	$\pi/3$
0	0	0	1	0	1	$\overline{V_{22}}$	$Vdc\sqrt{1/6}$	$2\pi/3$
0	0	0	1	0	1	$\overline{V_{23}}$	$Vdc\sqrt{1/6}$	π
0	0	0	0	0	1	$\overline{V_{24}}$	$Vdc\sqrt{1/6}$	$4\pi/3$
0	1	0	0	0	1	$\overline{V_{25}}$	$Vdc\sqrt{1/6}$	$5\pi/3$
0	1	0	1	0	1	$\overline{V_{26}}$	0	-
1	1	1	1	1	1	$\overline{V_{27}}$	0	-

In direct torque control, two hysteresis controllers are used to control the torque and flux, where the hysteresis levels are determined based on the available voltage vectors for control objectives. In the three-level diode-clamped inverter, there are 27 voltage vectors, and the conventional method utilizes 20 voltage vectors. To understand the operation of direct torque control, consider the (1) and (2). Equation (1) represents the torque relationship in a PMSM, and (2) is the derivative of (1) with respect to time. Equation (2) shows how torque variations affect the load angle and, consequently, how they influence the flux.

$$T_e = \frac{3P\lambda_s}{4L_dL_q}[2\lambda_m L_q \sin\delta + \lambda_s(L_d - L_q)\sin 2\delta] \quad (1)$$

$$\frac{dT_e}{dt} = \frac{3P\lambda_s}{4L_dL_q}[2\lambda_m L_q \cos\delta + \lambda_s(L_d - L_q)\cos 2\delta]\dot{\delta} \quad (2)$$

In this relationship, P represents the number of pole pairs, λ_s is the stator flux, Ld and Lq are direct- and the quadrature-axis inductances, λ_m magnitude of rotor flux linkages and δ is the angle between these two flux linkage vectors and its name is load angle.

These variations are achieved by changing the voltage vector. To further clarify this, consider Fig. 3. As seen in this figure, the voltage vector affects the flux value, load angle and consequently, the torque. Therefore, by utilizing different voltage vectors, various control states can be achieved.

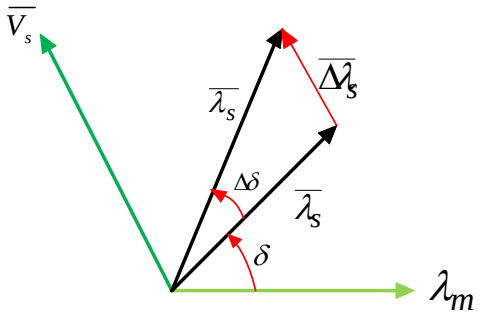

Fig. 3: Load angle and torque adjustment by voltage vectors.

According to Fig. 3, for example, it can be said that vector V4 causes torque control at its highest level, increasing both torque and flux, while vector V10 decreases the flux and controls the torque at its lowest level.

Therefore, the direct torque control table using the conventional method can be represented as shown in Table 3.

The hysteresis loops for torque and flux are given by (3) and (4).

$$\begin{cases} +3 \text{ for } 3\Delta T_e < T_{e_{error}} \\ +2 \text{ for } 2\Delta T_e \le T_{e_{error}} \le 3\Delta T_e \\ +1 \text{ for } \Delta T_e \le T_{e_{error}} \le 2\Delta T_e \\ 0 \text{ for } -\Delta T_e \le T_{e_{error}} \le \Delta T_e \\ -1 \text{ for } -2\Delta T_e \le T_{e_{error}} \le -\Delta T_e \\ -2 \text{ for } -3\Delta T_e \le T_{e_{error}} \le -2\Delta T_e \\ -3 \text{ for } T_{e_{error}} < -3\Delta T_e \end{cases} \quad (3)$$

$$\begin{cases} \varphi = 1 \text{ if } \lambda_{s_{error}} \ge \Delta\lambda/2 \\ \varphi = 0 \text{ if } \lambda_{s_{error}} < -\Delta\lambda/2 \end{cases} \quad (4)$$

B. The Proposed Method for DTC Using Voltage Vector and Virtual Voltage Vector

To further reduce the torque ripple, the number of hysteresis levels must increase.

To increase the number of hysteresis levels, the number of available voltage vectors for control in the desired regions must increase.

Table 3: Conventional look-up table of DTC

sector		1	2	3	4	5	6	7	8	9	10	11	12
λ	T												
1	+3	V4	V4	V6	V6	V8	V8	V10	V10	V12	V12	V2	V2
	+2	V3	V5	V5	V7	V7	V9	V9	V11	V11	V13	V13	V3
	+1	V15	V15	V16	V16	V17	V17	V18	V18	V19	V19	V14	V14
	0	V27	V1	V27	V1	V27	V1	V27	V1	V27	V1	V27	V1
	-1	V19	V19	V14	V14	V15	V15	V16	V16	V17	V17	V18	V18
	-2	V11	V13	V13	V3	V3	V5	V5	V7	V7	V9	V9	V11
	-3	V12	V12	V2	V2	V4	V4	V6	V6	V8	V8	V10	V10
0	+3	V6	V6	V8	V8	V10	V10	V12	V12	V2	V2	V4	V4
	+2	V5	V7	V7	V9	V9	V11	V11	V13	V13	V3	V3	V5
	+1	V16	V16	V17	V17	V18	V18	V19	V19	V14	V14	V15	V15
	0	V1	V27	V1	V27	V1	V27	V1	V27	V1	V27	V1	V27
	-1	V18	V18	V19	V19	V14	V14	V15	V15	V16	V16	V17	V17
	-2	V9	V11	V11	V13	V13	V3	V3	V5	V5	V7	V7	V9
	-3	V10	V10	V12	V12	V2	V2	V4	V4	V6	V6	V8	V8

In this paper, virtual voltages are used to increase the number of voltage vectors, such that a fixed duty cycle is defined for this controller, and in half the interval one voltage vector is used and in the other half duty cycle another voltage vector is used. To obtain the virtual vectors, the average vectors and half vectors are used, because the sum of the complete vectors has a value equal to the average vector and is collinear with it. The sum of the virtual vectors is obtained as follows:

$$\frac{1}{2}V_3+\frac{1}{2}V_5=0.61V_s\angle\frac{\pi}{3} \tag{5}$$

The virtual voltage vectors are obtained as shown in Table 4. Fig. 4 shows the distribution of these vectors in the αβ plane. Therefore, 12 voltage vectors are added to the control voltage vectors, and using these vectors, the hysteresis levels can be increased and an 11-level lookup table can be provided. The lookup table for switching the NPCI is presented as Table 5. The hysteresis levels in the proposed method are defined by (6) and (7).

$$\begin{cases}\varphi=1 \text{ if } \lambda_{s_{error}} \geq \Delta\lambda/2\\ \varphi=0 \text{ if } \lambda_{s_{error}} < -\Delta\lambda/2\end{cases} \tag{6}$$

$$\begin{cases}+5 \text{ for } T_{e_{error}} \geq 5\Delta T_e\\ +4 \text{ for } 4\Delta T_e \leq T_{e_{error}} \leq 5\Delta T_e\\ +3 \text{ for } 3\Delta T_e \leq T_{e_{error}} \leq 4\Delta T_e\\ +2 \text{ for } 2\Delta T_e \leq T_{e_{error}} \leq 3\Delta T_e\\ +1 \text{ for } \Delta T_e \leq T_{e_{error}} \leq 2\Delta T_e\\ 0 \text{ for } -\Delta T_e \leq T_{e_{error}} \leq \Delta T_e\\ -1 \text{ for } -2\Delta T_e \leq T_{e_{error}} \leq -\Delta T_e\\ -2 \text{ for } -3\Delta T_e \leq T_{e_{error}} \leq -2\Delta T_e\\ -3 \text{ for } -4\Delta T_e \leq T_{e_{error}} \leq -3\Delta T_e\\ -4 \text{ for } -5\Delta T_e \leq T_{e_{error}} \leq -4\Delta T_e\\ -5 \text{ for } T_{e_{error}} \leq -5\Delta T_e\end{cases} \tag{7}$$

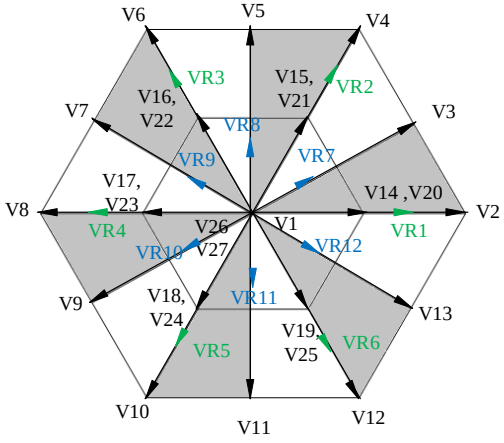

Fig. 4: Distribution of voltage vectors and virtual voltage vectors in the αβ plane.

DTC block diagram is shown in Fig. 5. In the next section, the simulation results will be examined in detail.

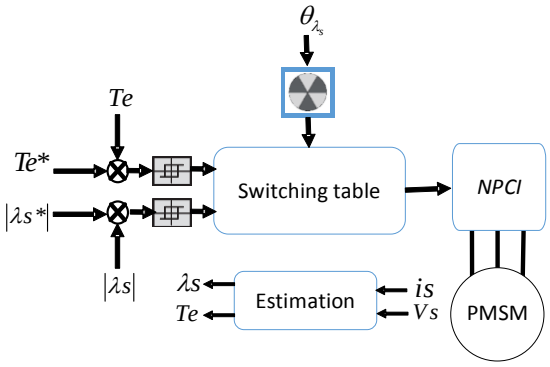

Fig. 5: Block diagram of DTC with proposed look-up table.

Table 4: Virtual vectors synthesis table

Virtual vector	Virtual vector	Sum of two voltage vector
VR1	V_3 , V_{13}	$0.61V_s\angle0$
VR2	V_3 , V_5	$0.61V_s\angle\frac{\pi}{3}$
VR3	V_5 , V_7	$0.61V_s\angle2\frac{\pi}{3}$
VR4	V_7 , V_9	$0.61V_s\angle\pi$
VR5	V_9 , V_{11}	$0.61V_s\angle-2\frac{\pi}{3}$
VR6	V_{11} , V_{13}	$0.61V_s\angle-\frac{\pi}{3}$
VR7	V20 , V21	$0.35V_s\angle\frac{\pi}{6}$
VR8	V21 , V22	$0.35V_s\angle\frac{\pi}{2}$
VR9	V22 , V23	$0.35V_s\angle5\frac{\pi}{6}$
VR10	V23, V24	$0.35V_s\angle7\frac{\pi}{6}$
VR11	V24 , V25	$0.35V_s\angle3\frac{\pi}{2}$
VR12	V25 , V20	$0.35V_s\angle11\frac{\pi}{6}$

C. *Smooth Vector Switching and Neutral-Point Voltage Balancing Control*

According to paper [30], whenever voltage vectors of large and small magnitudes are applied to the motor, neutral point oscillations occur. To prevent these oscillations, switching should be limited to adjacent vectors, adhering to the smooth voltage vector switching criterion. The hysteresis controller for flux control is a

two-level controller that oscillates between +1 and -1. Therefore, if the torque is continuously changing within the positive hysteresis band, for example, if the flux vector is also in the first region, according to the voltage vector switching table, the voltage vectors are adjacent to each other, and the voltage vector transition is from one vector to its adjacent vector. This approach ensures that the switching occurs between neighboring vectors, maintaining the smooth voltage vector switching principle and minimizing neutral point oscillations.

Furthermore, paper [26] states that the charge balance of DC link capacitors depends on the balance of the neutral point voltage. Therefore, if the neutral point voltage is zero, according to the following equations, the DC link capacitors are charged and discharged in a balanced manner:

$$i_o = i_{c1} - i_{c2} \tag{8}$$

$$\begin{cases} i_{c1} = c_1 \dfrac{dv_{c1}}{dt} \\ i_{c2} = c_2 \dfrac{dv_{c2}}{dt} \end{cases} \tag{9}$$

$$\begin{cases} V_{c1} = \dfrac{V_{dc}}{2} - v_o \\ V_{c2} = \dfrac{V_{dc}}{2} + v_o \end{cases} \tag{10}$$

$$i_o = -2C \frac{dv_o}{dt} \tag{11}$$

$$v_o = \frac{-1}{2C} \int i_o dt \tag{12}$$

Therefore, if the neutral point voltage equals zero, the neutral point balance is maintained, and the DC link capacitors are charged in a balanced manner.

Table 4: proposed look-up table of DTC

sector		1	2	3	4	5	6	7	8	9	10	11	12
λ	T												
	+5	V4	V4	V6	V6	V8	V8	V10	V10	V12	V12	V2	V2
	+4	V3	V5	V5	V7	V7	V9	V9	V11	V11	V13	V13	V3
	+3	V3+V5	V3+V5	V5+V7	V7+V5	V7+V9	V7+V9	V9+V11	V9+V11	V11+V13	V11+V13	V13+V3	V13+V3
	+2	V15	V15	V16	V16	V17	V17	V18	V18	V19	V19	V14	V14
	+1	V20+V21	V21+V22	V21+V22	V22+23	V22+23	V23+V24	V23+V24	V24+V25	V24+V25	V25+V20	V25+V20	V20+V21
1	0	V27	V1	V27	V1	V27	V1	V27	V1	V27	V1	V27	V1
	-1	V24+V25	V25+V20	V25+V20	V21+V20	V21+V20	V21+V22	V21+V22	V22+V23	V22+V23	V23+V24	V23+V24	V24+V25
	-2	V19	V19	V14	V14	V15	V15	V16	V16	V17	V17	V18	V18
	-3	V11+V13	V11+V13	V3+V13	V3+V13	V3+V5	V3+V5	V5+V7	V5+V7	V7+V9	V7+V9	V9+V11	V9+V11
	-4	V11	V13	V13	V3	V3	V5	V5	V7	V7	V9	V9	V11
	-5	V12	V12	V2	V2	V4	V4	V6	V6	V8	V8	V10	V10
	+5	V6	V6	V8	V8	V10	V10	V12	V12	V2	V2	V4	V4
	+4	V5	V7	V7	V9	V9	V11	V11	V13	V13	V3	V3	V5
	+3	V5+V7	V5+V7	V7+V9	V7+V9	V9+V11	V9+V11	V13+V11	V13+V11	V13+V3	V13+V3	V3+V5	V3+V5
	+2	V16	V16	V17	V17	V18	V18	V19	V19	V14	V14	V15	V15
	+1	V21+V22	V23+V22	V23+V22	V23+V24	V23+V24	V24+V25	V24+V25	V25+V20	V25+V20	V20+V21	V20+V21	V21+V22
0	0	V1	V27	V1	V27	V1	V27	V1	V27	V1	V27	V1	V27
	-1	V23+V24	V24+V25	V24+V25	V20+V25	V20+V25	V21+V20	V21+V20	V21+V22	V21+V22	V22+V23	V22+V23	V23+V24
	-2	V18	V18	V19	V19	V14	V14	V15	V15	V16	V16	V17	V17
	-3	V9+V11	V9+V11	V11+V13	V11+V13	V13+V3	V13+V3	V5+V3	V5+V3	V5+V7	V5+V7	V7+V9	V7+V9
	-4	V9	V11	V11	V13	V13	V3	V3	V5	V5	V7	V7	V9
	-5	V10	V10	V12	V12	V2	V2	V4	V4	V6	V6	V8	V8

Results and Discussion

To evaluate the feasibility of the proposed method, the conventional method and the proposed method were simulated in the MATLAB/Simulink environment, and the results are discussed in detail in this section. The parameters of the studied PMSM are observable in Table 6. It should be noted that both methods under study were simulated under the same conditions and with identical

motors. In this section, first, the steady-state results are studied, and then experiments entitled transient and no-load experiments are performed.

In the transient experiment, different speeds and loads were applied to the motor. In the no-load experiment, the motor started its operation from the unloaded condition, and then load variations were applied at a constant speed.

Fig. 6 shows the steady-state experiment. In this experiment, the motor was running at 180 rad/sec, and a torque of 4 N.m was applied to it.

Fig. 6(a) corresponds to the conventional method, and Fig. 6(b) corresponds to the proposed method. As observed, in the proposed method, the torque ripple is significantly lower than the conventional method, and the steady-state responses are as good as the conventional method.

Table 6: parameters of PMSM

Pole pair: Pn	4
Stator resistance: R_s	0.57Ω
d-axis inductance	8.72 mH
q-axis inductance	28.8 mH
Magnet flux linkage: $\boldsymbol{\lambda_m}$	0.108 wb
Vdc	310v

Fig. 7 shows the FFT analysis of the stator current, where Fig. 7(a) corresponds to the conventional method, and Fig. 7(b) corresponds to the proposed method. As observed, the stator current harmonics are significantly reduced compared to the conventional method, which is one of the advantages of the proposed method.

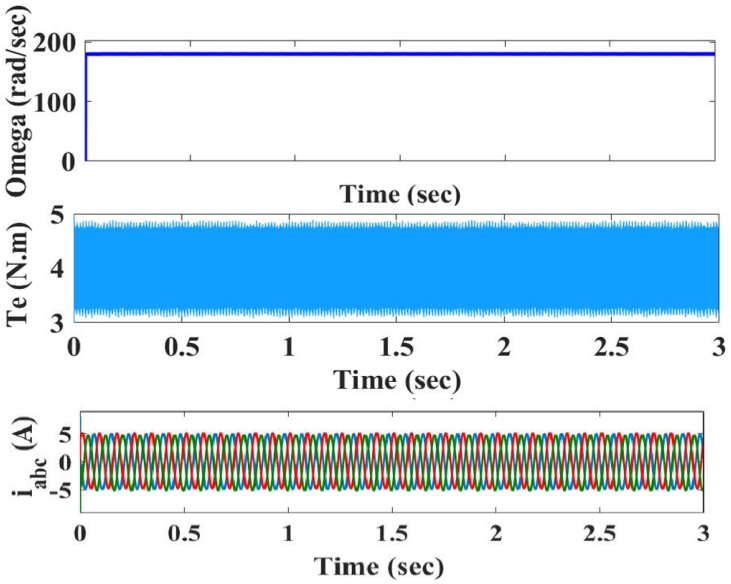

(a) Conventional methode

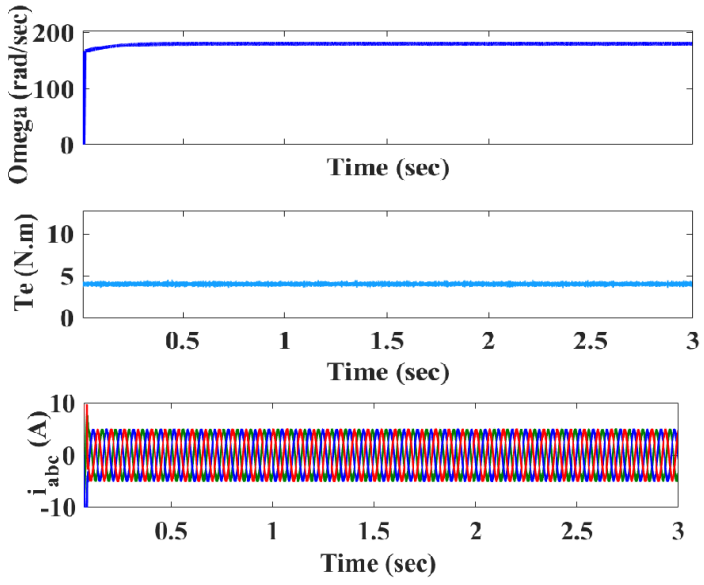

(b) Proposed methode

Fig. 6: Steady state performance. From top: speed, Torque & stator current.

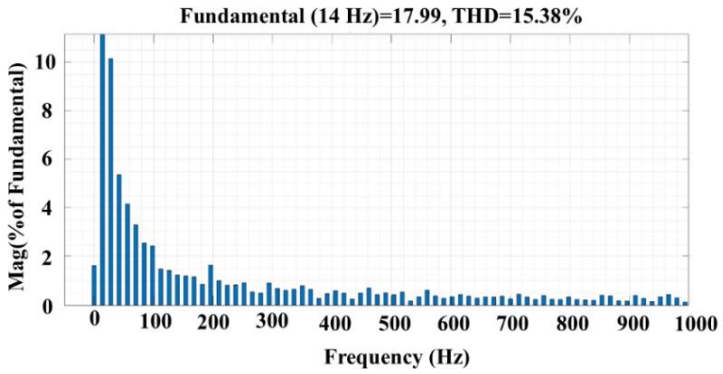

(a) Conventional methode

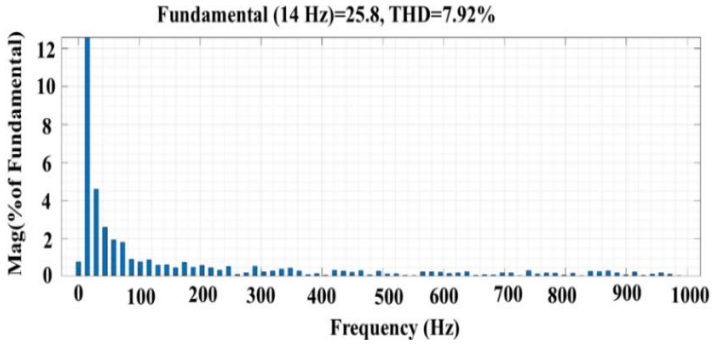

(b) Proposed methode

Fig. 7: FFT results of stator current.

Fig. 8 displays the motor experiment under transient conditions. In this experiment, the initial speed value was 188 rad/sec, and then it increased to 250 rad/sec in 1.5 sec. In this experiment, the torque value was also initially 1 N.m, which increased to 4 N.m in 1 sec and then decreased to 1 N.m in 2 sec. As observed, the transient results of the proposed method are as good as the conventional method.

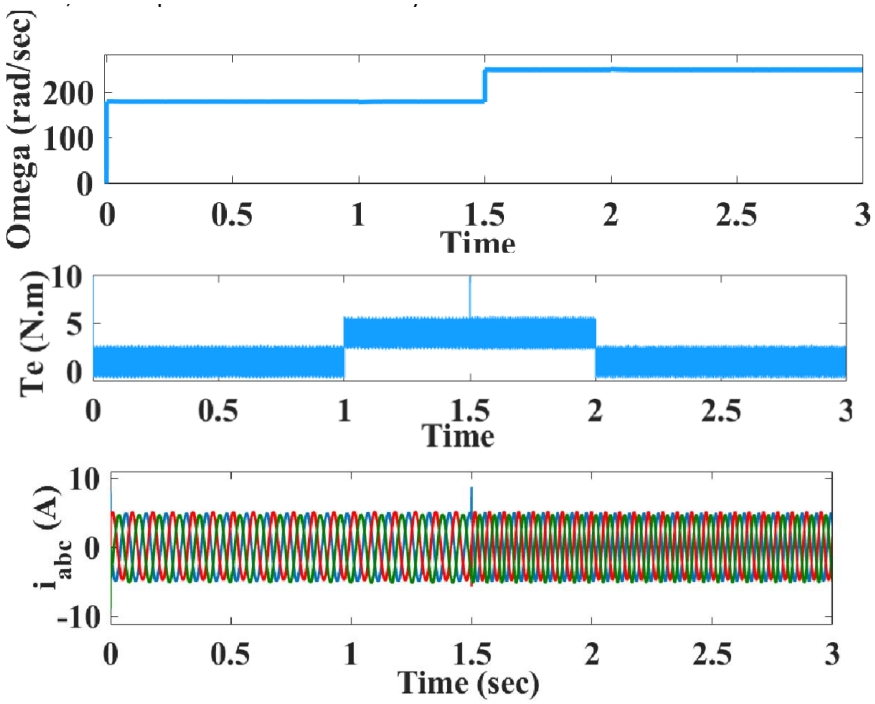

(a) Conventional methode

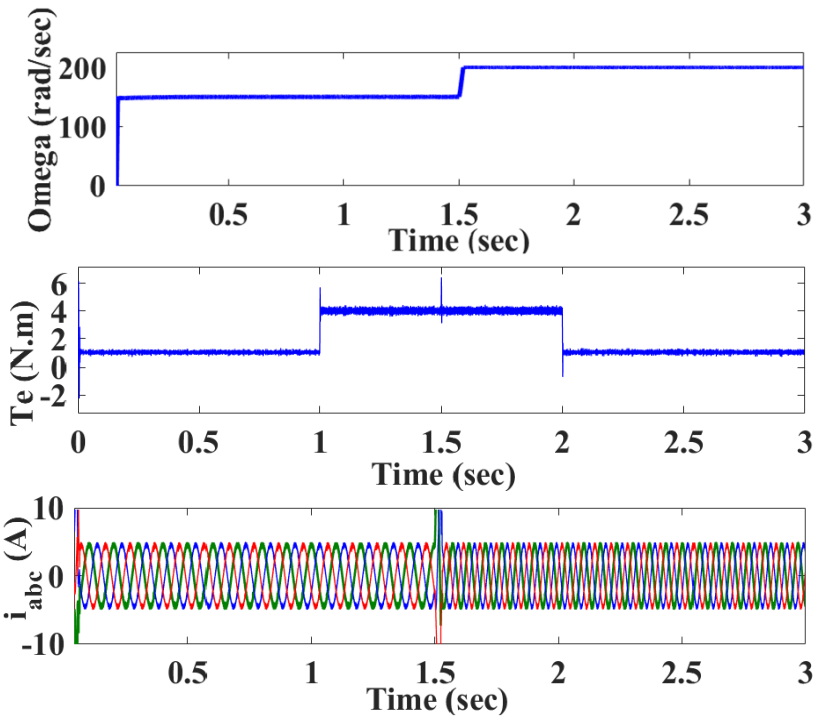

(b) Proposed methode

Fig. 8: Dynamic performance. From top: speed, Torque & stator current.

Fig. 9 shows the no-load test of the motor in simulation. In this test, the motor speed remains constant at 250 rad/sec, and the load torque increases from 0 N.m to 4 N.m and then returns to 0 N.m. In this experiment, it is observed that under load torque changes, the motor maintains its stability and follows the reference values.

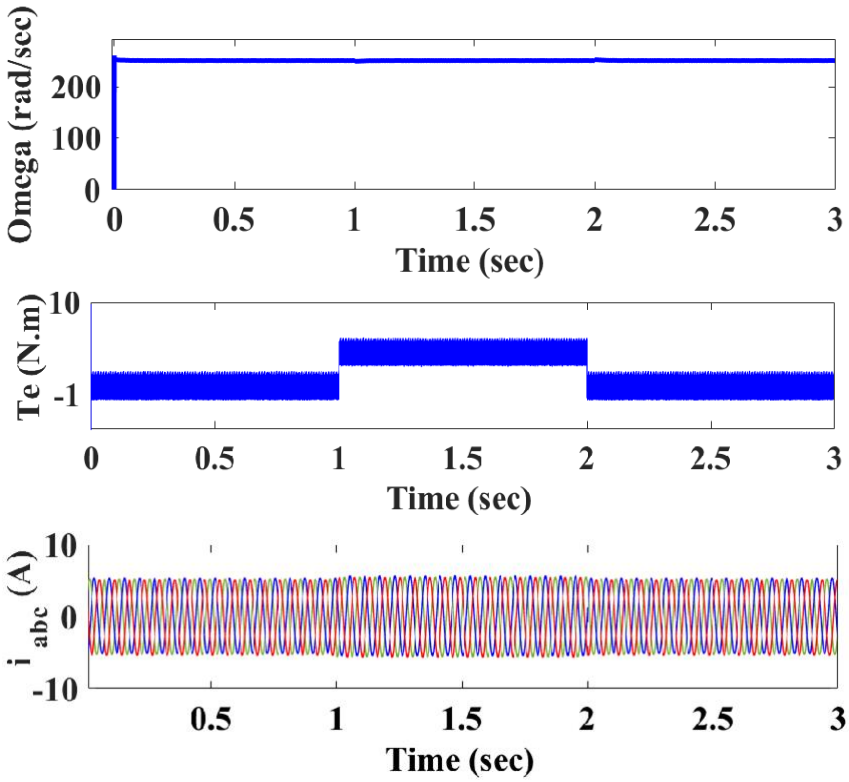

(a) Conventional methode

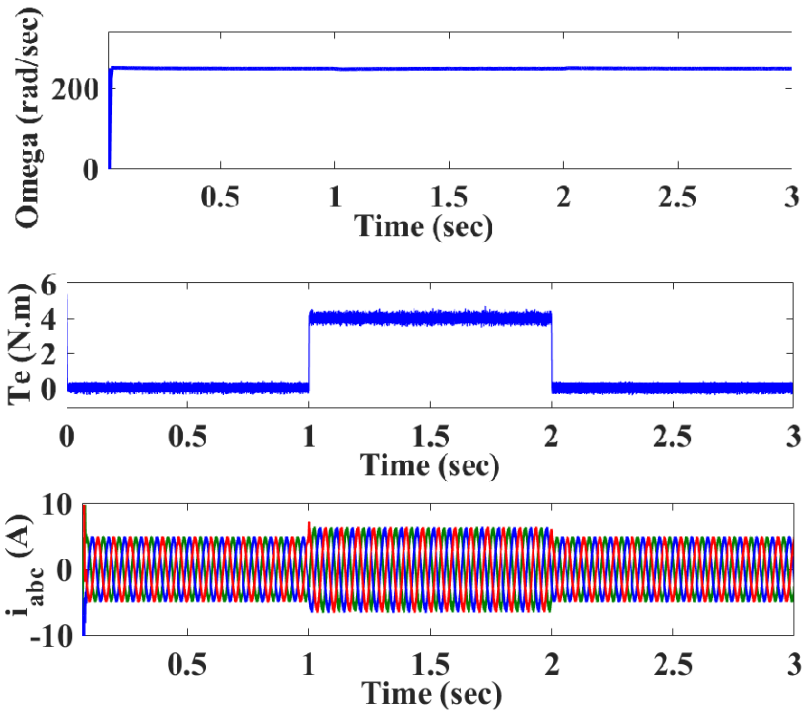

(b) Proposed methode

Fig. 9: Load disturbance. From top: speed, Torque & stator current.

Conclusion

In this paper, the DTC method is used for controlling a PMSM. In this controller, the motor is powered by a NPCI. NPCIs have 27 voltage vectors, but in the conventional method, only 20 voltage vectors are used for switching, and a maximum of 7 hysteresis levels can be defined. In the proposed method, virtual vectors are formed to increase the number of levels to reduce torque ripple and current harmonics. By forming virtual vectors, the problem of variable switching in the conventional method is solved, and the hysteresis levels are increased to 11 levels. The constant switching frequency leads to reduced losses and increased system efficiency. In the proposed method, the amount of torque ripple has decreased significantly, and current harmonics have also decreased. Another advantage of this method compared to modulation methods is the simplicity of the controller. Therefore, the proposed system provides an overall improvement over conventional method.

Author Contributions

This article is the result of a course project. H. Afsharirad provided critical supervision and expert guidance throughout the project, overseeing the research direction and ensuring the technical accuracy of the work. S.Misaghi was responsible for performing the simulations and drafting the initial manuscript. Both H.Afsharirad and S.Misaghi collaborated on analyzing the simulation results. The final manuscript was refined under the close supervision of H.Afsharirad.

Acknowledgment

The authors would like to thank the editor and anonymous reviewers.

Conflict of interest

The authors declare no potential conflict of interest regarding the publication of this work. In addition, the ethical issues including plagiarism, informed consent, misconduct, data fabrication and, or falsification, double publication and, or submission, and redundancy have been completely witnessed by the authors.

Abbreviations

NPCI	Neutral-Point-Clamped Inverter
DTC	Direct Torque Control
PMSM	Permanent magnet synchronous motor
PWM	Pulse Width Modulation

Reference

[1] J. Hyoung Ryu, K. W. Lee, J. S. Lee, "A unified flux and torque control method for DTC-based induction-motor drives," IEEE Trans. Power Electron., 21(1): 234-242, 2006.

[2] X. Chen, Z. Zhang, L. Yu, Z. Bian, "An improved direct instantaneous torque control of doubly salient electromagnetic machine for torque ripple reduction," IEEE Trans. Ind. Electron., 68(8): 6481-6492, 2021.

[3] P. Naganathan, S. Srinivas, "Direct torque control techniques of three-level h-bridge inverter fed induction motor for torque ripple

reduction at low-speed operations," IEEE Trans. Ind. Electron., 67(10): 8262-8270, 2020.

[4] K. B. Lee, S. H. Huh, J. Y. Yoo, F. Blaabjerg, "Performance improvement of DTC for induction motor-fed by three-level inverter with an uncertainty observer using RBFN," IEEE Trans. Energy Convers., 20(2): 276-283, 2005.

[5] E. P. Sarika, R. S. P. Raj, "Performance comparison of direct torque control of two level and three level neutral point clamped inverter fed three phase induction motor," in Proc. 2014 International Conference on Advances in Green Energy (ICAGE): 179-183, 2014.

[6] K. Tian, B. Wu, M. Narimani, D. Xu, Z. Cheng, N. Reza Zargari, "A capacitor voltage-balancing method for Nested Neutral Point Clamped (NNPC) inverter," IEEE Trans. Power Electron., 31(3): 2575-2583, 2016..

[7] S. E. Daoudi, L. Lazrak, M. A. Lafkih, "Sliding mode approach applied to sensorless direct torque control of cage asynchronous motor via multi-level inverter," Prot. Control Mod. Power Syst., 5(2): 1-10, 2020.

[8] G. H. B. Foo, T. Ngo, X. Zhang, M. F. Rahman, "SVM direct torque and flux control of three-level simplified neutral point clamped inverter fed interior PM synchronous motor drives," IEEE/ASME Trans. Mech., 24(3): 1376-1385, 2019.

[9] O. Chandra Sekhar, K. Chandra sekhar, "A novel five-level inverter topology for DTC induction motor drive," in Proc. 2012 IEEE International Conference on Advanced Communication Control and Computing Technologies (ICACCCT): 392-396, 2012.

[10] Z. Wang, X. Wang, J. Cao, M. Cheng, Y. Hu, "Direct torque control of T-NPC inverters-Fed double-stator-winding PMSM drives with SVM," IEEE Trans. Power Electron., 33(2): 1541-1553, 2018.

[11] P. Naganathan, S. Srinivas, "Direct torque control techniques of three-level h-bridge inverter fed induction motor for torque ripple reduction at low-speed operations," IEEE Trans. Ind. Electron., 67(10): 8262-8270, 2020.

[12] N. Babu A, P. Agarwal, "Nearest and non-nearest three vector modulations of NPCI using two-level space vector diagram—a novel approach," IEEE Trans. Ind. Appl., 54(3): 2400-2415, 2018.

[13] F. Faraji, A. A. M. Birjandi, S. M. Mousavi G, J. Zhang, B. Wang, X. Guo, "An improved multilevel inverter for single-phase transformerless PV system," IEEE Trans. Energy Convers., 36(1): 281-290, 2021.

[14] X. Wang, Z. Wang, M. Cheng, Y. Hu, "Remedial strategies of T-NPC three-level asymmetric six-phase PMSM drives based on SVM-DTC," IEEE Trans. Ind. Electron., 64(9): 6841-6853, 2017.

[15] S. Kouro et al., "Recent advances and industrial applications of multilevel converters," IEEE Trans. Ind. Electron., 57(8): 2553-2580, 2010.

[16] T. Geyer, S. Mastellone, "Model predictive direct torque control of a five-level anpc converter drive system," IEEE Trans. Ind. Appl., 48(5): 1565-1575, 2012.

[17] Z. Wang, X. Wang, J. Cao, M. Cheng, Y. Hu, "Direct torque control of T-NPC inverters-fed double-stator-winding PMSM drives with SVM," IEEE Trans. Power Electron., 33(2): 1541-1553, 2018.

[18] S. Payami, R. K. Behera, A. Iqbal, "DTC of three-level NPC inverter fed five-phase induction motor drive with novel neutral point voltage balancing scheme," IEEE Trans. Power Electron., 33(2): 1487-1500, 2018.

[19] D. Mohan, X. Zhang, G. H. B. Foo, "A simple duty cycle control strategy to reduce torque ripples and improve low-speed performance of a three-level inverter fed DTC IPMSM drive," IEEE Trans. Ind. Electron., 64(4): 2709-2721, 2017.

[20] P. Kant, B. Singh, "A sensorless DTC scheme for 60-pulse AC-DC converter fed 5-level six-leg NPC inverter based medium voltage induction motor drive," IEEE Trans. Energy Convers., 35(4): 1916-1925, 2020.

[21] A. Ramprasad, D. Giribabu, S. K. Kakodia, A. K. Panda, "Performance analysis of three-level NPC inverter Fed PMSM drives," in Proc. 2022 IEEE International Students' Conference on Electrical, Electronics and Computer Science (SCEECS): 1-6, 2022.

[22] D. Mohan, X. Zhang, G. H. B. Foo, "Three-level inverter-fed direct torque control of IPMSM with torque and capacitor voltage ripple reduction," IEEE Trans. Energy Convers., 31(4): 1559-1569, 2016.

[23] I. M. Alsofyani, K. B. Lee, "Improved predictive torque control with unidirectional voltage vector selection of PMSM fed by three-level neutral-point-clamped inverter," in Proc. 2023 IEEE International Symposium on Sensorless Control for Electrical Drives (SLED): 1-6, 2023.

[24] X. Jiang, Y. Wang, J. Dong, "Speed regulation method using genetic algorithm for dual three-phase permanent magnet synchronous motors," CES Trans. Electr. Mach. Syst., 7(2): 171-178, 2023.

[25] J. Shen, X. Wang, D. Xiao, Z. Wang, Y. Mao, M. He, "Online switching strategy between dual three-phase PMSM and open-winding PMSM," IEEE Trans. Transp. Electrif., 10(1): 1519-1529, 2024.

[26] O. Sandre Hernandez, J. Rangel Magdaleno, R. Morales Caporal, E. Bonilla Huerta, "HIL simulation of the DTC for a three-level inverter fed a PMSM with neutral-point balancing control based on FPGA," Electr. Eng., 100: 1441-1454, 2018.

[27] S. G. Petkar, V. K. Thippiripati, "A novel duty-controlled DTC of a surface PMSM drive with reduced torque and flux ripples," IEEE Trans. Ind. Electron., 70(4): 3373-3383, 2023.

[28] Y. Liu et al., "Direct torque control schemes for dual three-phase PMSM considering unbalanced DC-Link voltages," IEEE Trans. Energy Convers., 39(1): 229-242, 2024.

[29] T. Yuan, D. Wang, X. Wang, X. Wang, Z. Sun, "High-precision servo control of industrial robot driven by PMSM-DTC utilizing composite active vectors," IEEE Access, 7: 7577-7587, 2019.

[30] T. A. Huynh, Y. T. Nguyen Le, Z. Lee, M. C. Tsai, P. W. Huang, M. F. Hsieh, "Influence of Flux barriers and permanent magnet arrangements on performance of high-speed flux-intensifying IPM Motor," IEEE Trans. Magn., 59(11): 1-6, 2023.

Biographies

Hadi Afsharirad was born in Abhar, Iran, in 1985. He received the B.Sc. degree from the Zanjan University, Iran and M.Sc. and Ph.D. degrees, from the University of Tabriz, Tabriz, Iran, in 2008, 2010, and 2018, respectively, all in Electrical Engineering. He is an Assistant Professor with the Department of Electrical Engineering, Azarbaijan Shahid Madani University, Tabriz, which he joined in 2020. His main research interests include the electric and hybrid electric vehicles, renewable energy, linear electric machines and electrical drives.

- Email: h.afsharirad@azaruniv.ac.ir
- ORCID: 0009-0005-6259-7855
- Web of Science Researcher ID: LNR-5960-2024
- Scopus Author ID: 36670802500
- Homepage: hppts://pajouhesh.azaruniv.ac.ir/_Pages/Researcher.aspx?ID=8492

Sara Misaghi was born in Iran, in 1997. She received the B.Sc. and M.Sc. degree from the Azarbaijan Shahid Madani University, Iran. Her main research interests include electric machines and Electrical Drives.

- Email: sara.misaghi@azaruniv.ac.ir
- ORCID: 0009-0002-0145-4461
- Web of Science Researcher ID: LNR-6161-2024
- Scopus Author ID: NA
- Homepage: https://pajouhesh.azaruniv.ac.ir/_Pages/Researcher.aspx?ID=12999

How to cite this paper:
H. Afsharirad, S. Misaghi, "Torque ripple reduction by using virtual vectors in direct torque control method using neutral-point-clamped inverter," J. Electr. Comput. Eng. Innovations, 13(1): 197-208, 2025.

DOI: 10.22061/jecei.2024.10894.745

URL: https://jecei.sru.ac.ir/article_2227.html